# Phase-amplitude-phase modulation for arbitrary impedance matrices implemented with adjustable acoustic metasurface

Yu-Ze Tian,[1] Zhuo-Run Wei,[2] Yan-Feng Wang,[1,3,*] Vincent Laude,[4] and Yue-Sheng Wang[1,5]

[1] *School of Mechanical Engineering, Tianjin University, 300350 Tianjin, China*
[2] *School of Science, Tianjin University, 300350 Tianjin, China*
[3] *National Key Laboratory of Vehicle Power System, 300350 Tianjin, China*
[4] *Université de Franche-Comté, CNRS, Institut FEMTO-ST, F-25000 Besançon, France*
[5] *Institute of Engineering Mechanics, Beijing Jiaotong University, Beijing 100044, China*

Impedance metasurfaces enable accurate regulation of acoustic fields. However, their perfect operation is accompanied by rigorous requirements on the design of unit cells. Actually, an arbitrary lossless and passive target impedance matrix requires the tuning of three independent real parameters. The set composed of a reflection phase, a transmission amplitude and a transmission phase, enables the representation of an arbitrary impedance matrix, possibly possessing singular elements. In this paper, the principle of phase-amplitude-phase modulation (PAP modulation) is introduced for the generic design of the unit cells of acoustic impedance metasurfaces. Adjustable acoustic impedance metasurfaces are further available under this framework. An impedance unit with three mobile parts is designed based on this idea. The assembled metasurface can handle different incidences for acoustic field manipulation at a given frequency. Beam steering and beam splitting are considered as demonstration examples and are verified by numerical simulation and experiment. PAP modulation enriches the design of acoustic impedance metasurfaces and extends the range of application of impedance theory.

**Keywords**: Impedance theory; Adjustable acoustic metasurfaces; Precise wave steering; Precise beam splitting

Acoustic metasurfaces, a sub-set of acoustic metamaterials [1–5], have aroused great interest these days. they greatly facilitate wave field manipulation through compact structural design. Several theoretical approaches have been proposed to sustain this concept [6–9]. The recently proposed impedance theory, that is now attracting wide attention, imposes strict power flow conservation, in contrast to former approaches [10–12]. Various functions have been implemented rigorously with acoustic impedance metasurfaces, for instance beam steering [11], beam splitting [13, 14], orbital angular momentum generation [15], plane-cylinder wave conversion [16–18], and encrypted information storage [19].

Impedance theory was first proposed in electromagnetism, with the benefit that parasitic scattering can be eliminated provided the boundary impedance is rationally tailored [10]. Transplanted to acoustics by Díaz-Rubio et al. [11], impedance models for both reflective and refractive metasurfaces were established. A reflective impedance metasurface with simple slot units was in particular designed. Non-local power flow, however, seemed hardly avoidable due to the occurence of real values in the boundary impedance. In order to reduce complexity, curved metasurfaces were then investigated under a power flow conformal strategy, using similar slot units [20]. Bending the metasurface in the light of the distribution of the power flow enabled the boundary impedance to remain purely imaginary. The resulting metasurface could then be designed independently with a discretized structure of elementary unit cells. Li et al. proposed a structure with Helmholtz resonators for the design of refractive metasurfaces [21]. With this solution, the impedance matrix of the interface can be approached by independent unit cells composed of four cascaded resonators with inhomogeneous sound capacities. This approach was later generalized by Tian et al. [14] within the framework of integral equivalence. Actually, it can be proven that any pair of acoustic fields can be passively connected as long as global power flow conservation is imposed.

Nonetheless, there is so far no clear solution to design a structure implementing an arbitrary impedance matrix, especially in the case of transmission metasurfaces. Helmholtz resonator units may cover a certain range of impedance matrices [21], but it remains difficult to infer without resorting to optimization what geometric parameters are sufficient for achieving a target impedance matrix. In addition, although impedance theory is in principle as functional as the generalized Snell's law is, it somehow lacks its flexibility. Once the impedance metasurface is fabricated, indeed, the incident and the reflected or refracted wave fields are fully determined [19]. Perfect power flow manipulation hence can only be observed under preset operating conditions. The requirement on a flexible response cannot be fulfilled by the current Helmholtz resonators, as well. Adjustable structures like those based on the generalized Snell's law [22–28] are desirable so that the impedance matrix can be adjusted according to the target function, which has not been achieved yet.

In this paper, the principle of phase-amplitude-phase modulation (PAP modulation) is proposed for the design of unit cells of acoustic impedance metasurfaces. It

* wangyanfeng@tju.edu.cn

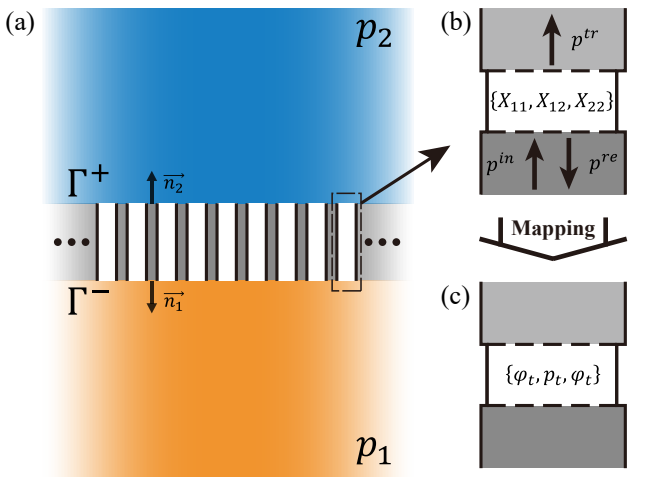


FIG. 1. Schematic representation of impedance theory. (a) An impedance metasurface connecting two acoustic fields $p_1$ and $p_2$ is discretized into unit cells for design purposes. Adjacent unit cells are rigidly isolated to avoid crosstalk. (b) The impedance components $\{X_{11}, X_{12}, X_{22}\}$ of each unit cell can be monitored independently under plane wave incidence. (c) After establishing the mapping between the impedance matrix $Z = \imath X$ and the transmission and reflection coefficients, impedance unit cells are characterized by the real triplet $\{\varphi_r, p_t, \varphi_t\}$.

is first argued that the number of independent design parameters is three. It is proved that any conservative impedance matrix can be approached by modulating the transmitted and reflected waves from one side. Based on this idea, an adjustable unit with two phase modulators and an amplitude modulator is designed. The assembled metasurface provides target wave manipulation under different incidence angles at a given frequency. Beam steering with two different operation angles and beam splitting are demonstrated by numerical simulation based on impedance theory. Scattering is almost undetectable in all three considered scenarios. Two groups of samples are fabricated and show nearly perfect experimental operation.

We start by recalling certain essential results on impedance unit cells of acoustic metasurfaces. Generally, a transmission metasurface is regarded as the connection between two acoustic fields $p_1$ and $p_2$, each obeying a scalar Helmholtz equation [21], as shown in Fig. 1(a). A passive and lossless impedance matrix is expressed as

$$\begin{bmatrix} p_1 \\ p_2 \end{bmatrix} = \imath \begin{bmatrix} X_{11} & X_{12} \\ X_{21} & X_{22} \end{bmatrix} \begin{bmatrix} -\mathbf{n}_1 \cdot \mathbf{v}_1 \\ -\mathbf{n}_2 \cdot \mathbf{v}_2 \end{bmatrix} \text{ on } \Gamma, \tag{1}$$

where $\imath$ is imaginary unit, $\mathbf{v}_i$ is the local velocity, and $\mathbf{n}_i$ is the normal vector to the interface entering the region ($i = 1, 2$). Diagonal components must be equal, $X_{12} = X_{21}$, to ensure the continuity of normal power flow [19]. Unit cells arise from the discretization of the metasurface and each supply a specific impedance matrix determined by its spatial position and Eq. (1). Adjacent units should be rigidly isolated to ensure the absence of crosstalk and hence independent design. The tangential dimension must be deeply sub-wavelength, so that there is only one mode of propagation inside the unit cell at a given frequency. As a consequence, the impedance matrix $Z = \imath X$ is defined uniquely under any excitation and can be detected by coupling into a waveguide [13].

The unit cell is described by a set of three independent variables, e.g. $\{X_{11}, X_{12}, X_{22}\}$. assigning an obvious physical meaning to these impedance elements is however not immediate. Instead, from the set of incident, transmitted and reflected waves ($p^{in}$, $p^{tr}$ and $p^{re}$ in Fig. 1(b)) [14], the impedance matrix can be written

$$\begin{aligned} X &= \begin{bmatrix} X_{11} & X_{12} \\ X_{21} & X_{22} \end{bmatrix} \\ &= \frac{Z_0}{D} \begin{bmatrix} \cos\varphi_t + \frac{p_r}{p_i}\cos(\varphi_r - \varphi_t) & \frac{p_i^2 - p_r^2}{p_t p_i} \\ \frac{p_t}{p_i} & \cos\varphi_t - \frac{p_r}{p_i}\cos(\varphi_r - \varphi_t) \end{bmatrix} \end{aligned} \tag{2}$$

$$D = \frac{p_r}{p_i}\sin(\varphi_r - \varphi_t) + \sin\varphi_t, \tag{3}$$

where $p_i$, $p_t$ and $p_r$ are the amplitudes of incident, transmitted and reflected waves, respectively, $\varphi_r$ and $\varphi_t$ are the reflection and transmission phases referred to the incident wave, and $Z_0$ is the characteristic impedance of the background medium. $X_{12}$ and $X_{21}$ are equal under the condition of power flow conservation, $p_i^2 = p_r^2 + p_t^2$. The set of three independent real quantities $\{\varphi_r, p_t, \varphi_t\}$ can be taken as representative of the impedance matrix. Furthermore, an inverse mapping is

$$\begin{aligned} \frac{p_r}{p_i} e^{\imath\varphi_r} &= \frac{(\imath X_{11} - Z_0)(\imath X_{22} + Z_0) + X_{12}X_{21}}{(\imath X_{11} + Z_0)(\imath X_{22} + Z_0) + X_{12}X_{21}}, \\ \frac{p_t}{p_i} e^{\imath\varphi_t} &= \frac{2\imath X_{12} Z_0}{(\imath X_{11} + Z_0)(\imath X_{22} + Z_0) + X_{12}X_{21}}. \end{aligned} \tag{4}$$

Accordingly, there is always a unique couple of complex transmission and reflection coefficients for any impedance matrix.

The mapping above provides us with an opportunity to characterize the impedance matrix using $\{\varphi_r, p_t, \varphi_t\}$, as shown in Fig. 1(c). An arbitrary impedance matrix can be therefore be achieved uniquely by simply modulating the amplitudes and phases of the transmitted and reflected waves, excited from one side of the metasurface. As a consequence, unit cell design can be decoupled into three structures that supply independent modulation on the reflection phase, the reflection/transmission amplitude, and the transmission phase. We name such a structure phase-amplitude-phase modulation (PAP modulation) of the impedance matrix.

Interestingly, even singular impedance matrices fall under this framework. For instance, the impedance matrice is singular if $\varphi_t = m\pi$ ($m \in \mathbb{Z}$) with no reflection ($p_r = 0$). At this point, the impedance unit actually

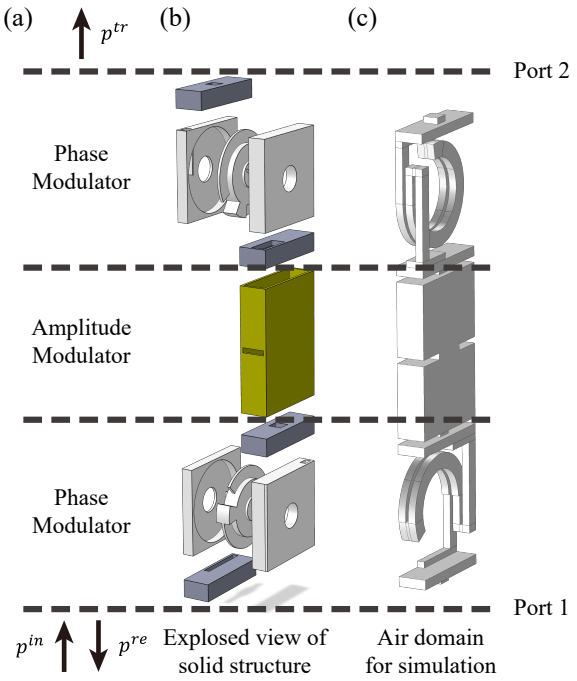


FIG. 2. Schematic representation of the designed adjustable acoustic impedance unit: (a) PAP modulation: (b) exploded view of the solid structure consisting of two phase modulators (white parts) with four resonators (gray parts) and one amplitude modulator (yellow part), (c) air domain considered in numerical simulations.

provides a phase difference of $\pi$ or nothing but continuity, which can be easily achieved by a phase modulator. Another special case is $\varphi_t = m\pi\,(m \in \mathbb{Z})$ with $\varphi_r - \varphi_t = n\pi\,(n \in \mathbb{Z})$. The impedance matrix is then singular as well. This situation can perfectly occur with PAP modulation.

In contrast to the previous design of four series-connected Helmholtz resonators [21], only three sections are required for PAP modulation, as shown in Fig. 2(a). One can easily design a structure with a specific impedance matrix by connecting two phase modulators through an amplitude modulator. Ideally, the transmission and reflection amplitudes would be uniquely controlled by the amplitude modulator when designing the two phase modulators to have a perfect transmittance [29]. The reflection phase is controlled by the lower phase modulator and the transmission phase is jointly controlled by both phase modulators. The selection of the structural geometry is made easier, as there exist abundant structures supplying a phase shift with a complete transmission [30, 31] while the amplitude modulator can be regarded as a simple insertion. Theoretically, impedance unit cells can be made ultrathin as well if they are based on the idea of space coiling [32, 33], but the latter choice is not compulsory.

Furthermore, adjustable acoustic impedance metasurfaces are available under the concept of PAP modulation. A unit cell with three adjustable parts is designed as an example. The operating frequency is selected as $f_0 = 3500$ Hz, or wavelength in air $\lambda_0 = c_0/f_0 = 9.8$ cm. The tangential dimension of the unit cells is $d_u = 1.12$ cm, or about $\lambda_0/9$. The exploded view is depicted in Fig. 2(b) (see Supplementary Note 1 for details of the optimized geometry and transmission characteristics of the designed unit). Two phase modulators (white parts) are images in a central symmetry and are connected through an amplitude modulator (yellow part). Two resonators (gray parts) are connected in series at both ends of each phase modulator. High transmittance for phase difference modulation is guaranteed by optimization of the two resonators. The propagation distance (the air domain in Fig. 2(c)) changes accordingly when rotating the middle knob. The modulators can then support linear and continuously adjustable phase differences. The amplitude modulator, located between the two phase modulators, is a cuboid cavity with a central opening for insertion (not drawn for simplicity). The amplitude of transmittance can be modulated by changing the cavity depth. The reflection phase for waves incident from below is uniquely controlled by the lower modulator, while the transmission phase is jointly controlled by both modulators. The array direction of unit cells is perpendicular to the rotation plane of the knob. The upper and lower ports are connected to the acoustic fields directly.

Three cases are examined next to check the operation of the designed unit cells when assembling a metasurface. Twenty unit cells are arrayed together with repetition distance $D = 20d_u$. The case of beam steering under normal incidence ($\theta_i = 0°$) is demonstrated first. The refraction angle is set to $\theta_t = +26°$. The continuously varying impedance elements are plotted as solid lines in Fig. 3(a). Twenty sampling points (circles in Fig. 3(a)) are uniformly selected with an interval of $d_c$ for numerical simulation by the three-layer numerical model [11]. Results are shown in Fig. 3(b) (see Supplementary Note 2 for a detailed calculation of interface impedance and a description of the settings in numerical simulations). It can be observed that almost all power is redirected toward the target direction. Limited spurious scattering occurs due to discretization of unit cells.

Unit cells are then adjusted to approach the required impedance matrix with the help of optimization. The rotation angles of the knobs in the two phase modulator and the depth of the insertion in the amplitude modulator can then be obtained (see Supplementary Note 3 for detailed parameters). The impedance provided by the designed structure is plotted with square points in Fig. 3(a). Assembling the unit cells into a metasurface, finite element analysis (FEA) of wave transmission is presented in Fig. 3(c). Little degradation is observed compared with the three-layer numerical model.

Beam steering with large refraction angles is in principle an advantage of metasurfaces based on impedance theory compared to those based on the generalized Snell's law [11]. A transmission angle $\theta_t = -70°$ under an in-

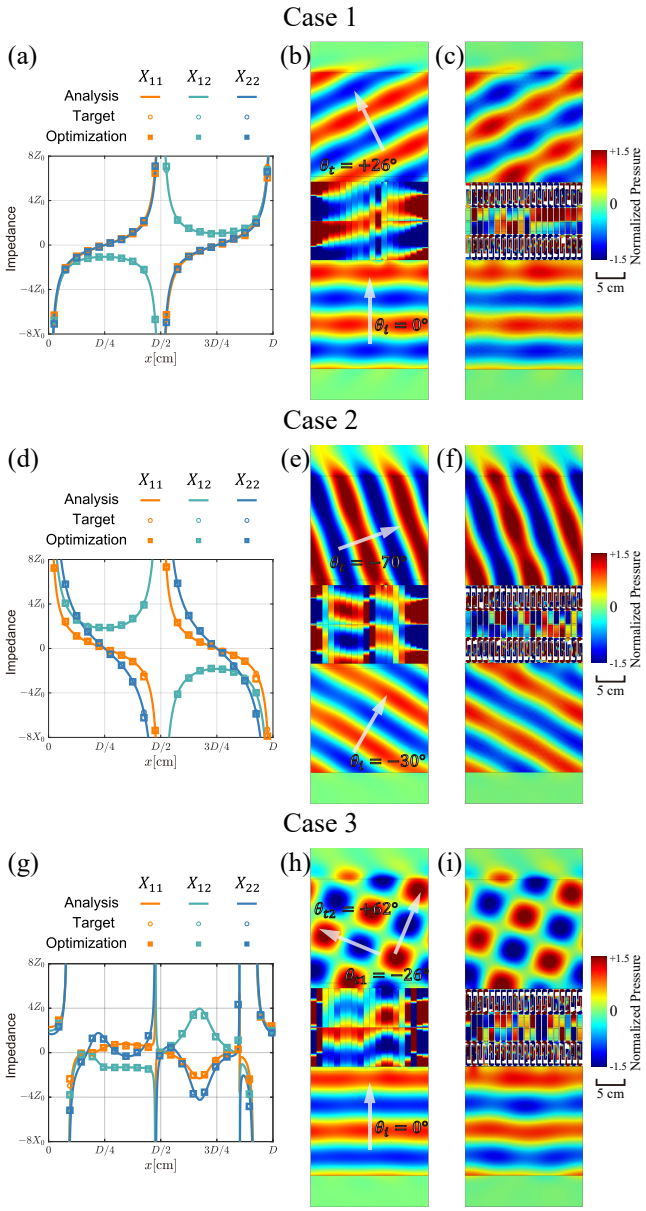


FIG. 3. Numerical simulation of adjustable impedance metasurfaces. Case 1: (a) interface impedance, (b) simulation by 2D three-layer model and (c) simulation by 3D FEA for beam steering with $\theta_i = 0°$ and $\theta_t = +26°$. Case 2: (d) interface impedance, (e) simulation by 2D three-layer model and (f) simulation by 3D FEA for beam splitting with $\theta_i = -30°$ and $\theta_t = -70°$. Case 3: (g) interface impedance, (h) simulation by 2D three-layer model and (i) simulation by 3D FEA for beam splitting with $\theta_i = 0°$, $\theta_{t1} = +62°$ and $\theta_{t2} = -26°$.

cidence angle of $\theta_i = -30°$ is considered as an example. The interface impedance provided by theoretical analysis is shown in Fig. 3(d), together with the result of the optimization of the unit cells. The adjustable impedance metasurface approaches the target impedance successfully. Numerical simulation of the acoustic fields by the three-layer model and FEA are shown in Fig. 3(e) and (f). Beam steering at a large angle is obtained with limited spurious scattering.

The case of beam splitting is considered next to illustrate the versatility of the design. It is known the impedance theory supports perfectly splitted beams with different angles [13], in contrast to the generalized Snell's law [34, 35]. Two splitted beams are targeted under normal incidence with the same amplitudes and transmission angles $\theta_{t1} = +62°$ and $\theta_{t2} = -26°$. The required impedance distribution is more complex than for a single output beam, as shown in Fig. 3(g). The interface impedances provided by the adjustable units, anyway, still coincides with the target values. Satisfying operation is obtained in numerical simulations by the three-layer numerical model [Fig. 3(h)] and FEA [Fig. 3(i)] (see Supplementary Note 3 for a quantitative evaluation for all three cases).

We emphasize that the complete set of impedance matrices, and not the local transmission and reflection coefficients, is required to evaluate the performance of the adjustable unit cell, although the latter is approached locally through PAP modulation. This is because both reflected and transmitted fields are actually controlled by the interface impedance provided by the whole metasurface [see Eq. (1)]. The local transmittance of a particular unit cell does not have a significant impact on the entire wave field in the framework of impedance theory. As an example, the interface impedance of the metasurface designed for anomalous refraction corresponds to a scattering matrix with component $|S_{12}| \leq 1$. This indicates that the unit cells that compose this metasurface always show a local transmittance that is less than 1 (see Supplementary Note 2 for a detailed proof). However, they collectively provide the required impedance relationship of Eq. (1) at the boundary, stably connecting the preset incident and transmitted fields. As a result, manipulation of the transmitted field remains perfect as shown in Fig. 3.

Moreover, the uniform width of the unit cells of the metasurfaces exhibited in this paper is only chosen for convenience. The assembled metasurface always provides perfect wave manipulation even if the width of unit cells is not uniform. The adaptability of impedance theory is therefore greatly promoted as different goals can be achieved under arbitrary incidence.

Experiments were conducted to validate the operation of the designed metasurfaces. Metasurface samples were fabricated by 3D printing, one period at a time for simplicity. Four periods are included in each metasurface during experiments. Photographs of the samples corresponding to Case 1 (beam steering) and Case 3 (beam splitting) are shown in Figs. 4(a) and (b). Each sample is composed of a main body with a thickness of 3.3 cm and a cover with a thickness of 0.2 cm introduced for convenience of manufacturing. Numerical simulations by FEA following experimental settings are presented in Figs. 4(c) and (d) for comparison purposes (see Supplementary Note 4 for detailed information about experi-

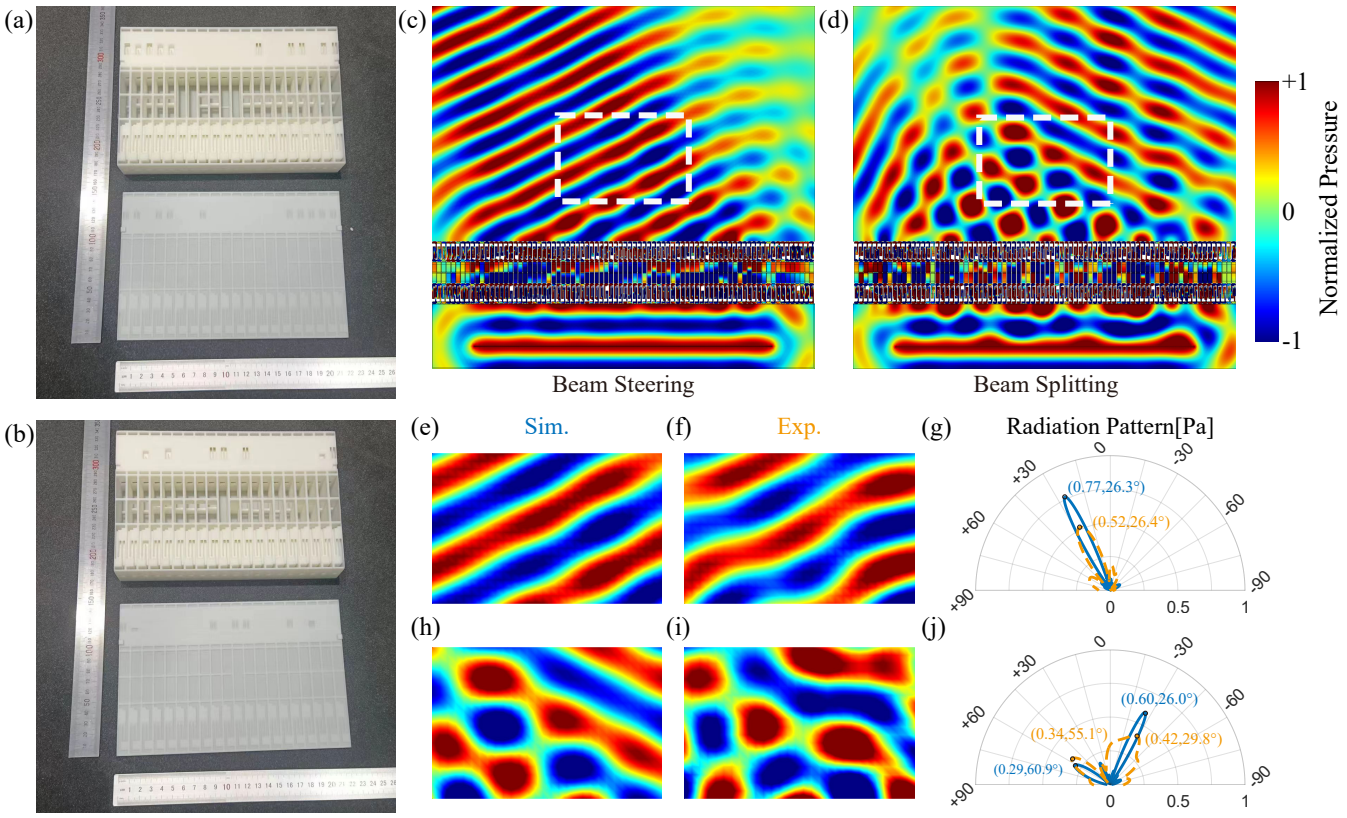


FIG. 4. Experimental verification of adjustable impedance metasurface. A period of the metasurface sample is shown for (a) Case 1 and (b) Case 3. Simulation results for (c) Case 1 and (d) Case 3 are given for the metasurface excited by a finite width beam. The acoustic field of Case 1 in the measured area is given for (e) numerical simulation and (f) experiment and (g) corresponding radiation pattern. The acoustic field of Case 3 in the measured area is given for (h) numerical simulation and (i) experiment and (j) corresponding radiation pattern.

ment). Close to perfect operation is observed visually in both cases. Some distortions occur at the edges of the refractive beam in Fig. 4(c) due to the limited width of the metasurface. The splitted beams in Fig. 4(d) share the same amplitude, as expected, although different transmission angles result in different beam widths.

Fig. 4 further provides close-up views at the acoustic fields. The region corresponding to the measurement area available during experiments is overlaid with a white dashed box in Figs. 4(c) and (d). The simulated pressure field of Case 1 is presented in Fig. 4(e), whereas the experimental pressure field is presented in Fig. 4(f). All color maps are normalized according to the average amplitude of the incident field. Good consistency is observed visually, except for some undesired disturbances in the experimental results. The radiation pattern is provided in Fig. 4(g) for quantitative evaluation (see Supplementary Note 4 for a detailed definition). It can be seen from the main lobe in Fig. 4(l) that the metasurface for beam steering provides a refraction angle of $\theta_t = 26°$ in both simulation and experiment. The amplitude of the main experimental lobe is reduced due to thermoviscous losses, but the beam direction is not affected significantly.

The situation is similar in the case of beam splitting shown in Figs. 4(h-i). It should be noted that the amplitudes of the spitted beams are not the same in the far field as shown in Fig. 4(j). This is owing to the difference in beam widths mentioned earlier. Their ratio is equal to the ratio of the cosine of splitting angle $\cos\theta_{t1}/\cos\theta_{t2}$. In general, there are only slight deviations in amplitude and direction in the experimental result.

In this paper, a method termed PAP modulation has been proposed for the design of the unit cells of adjustable acoustic impedance metasurfaces. It was proven that any impedance matrice can be approached by the modulation of transmission and reflection coefficients, with a total of three independent parameters. Each unit cell is composed of three mobile parts and can implement an arbitrary impedance matrix. Functions such as beam steering and beam splitting can be realized efficiently under arbitrary incidence. The operation was verified both by numerical simulation and experiment. Theoretically, stepless adjustment of beam steering and beam splitting could be achieved as well through automation control,

though the practical fabrication of adjustable structures might be a limitation as of today. More efficient and accurate manufacturing techniques will be the focus of future research. The work reported here is expected to enhance the versatility and applicability of acoustic impedance metasurfaces.

## ACKNOWLEDGMENTS

The authors acknowledge financial support by the National Natural Science Foundation of China 12072223, 12122207, 12021002 and 11991032). V.L. acknowledges financial support by the EIPHI Graduate School (ANR-17-EURE-0002).

[1] Steven A Cummer, Johan Christensen, and Andrea Alù. Controlling sound with acoustic metamaterials. *Nature Reviews Materials*, 1(3):1–13, 2016.

[2] Shuang Chen, Yuancheng Fan, Quanhong Fu, Hongjing Wu, Yabin Jin, Jianbang Zheng, and Fuli Zhang. A review of tunable acoustic metamaterials. *Applied Sciences*, 8(9):1480, 2018.

[3] Junyi Liu, Hanbei Guo, and Ting Wang. A review of acoustic metamaterials and phononic crystals. *Crystals*, 10(4):305, 2020.

[4] Yan-Feng Wang, Yi-Ze Wang, Bin Wu, Weiqiu Chen, and Yue-Sheng Wang. Tunable and active phononic crystals and metamaterials. *Applied Mechanics Reviews*, 72(4):040801, 2020.

[5] Guangxin Liao, Congcong Luan, Zhenwei Wang, Jiapeng Liu, Xinhua Yao, and Jianzhong Fu. Acoustic metamaterials: A review of theories, structures, fabrication approaches, and applications. *Advanced Materials Technologies*, 6(5):2000787, 2021.

[6] Badreddine Assouar, Bin Liang, Ying Wu, Yong Li, Jian-Chun Cheng, and Yun Jing. Acoustic metasurfaces. *Nature Reviews Materials*, 3(12):460–472, 2018.

[7] A-Li Chen, Yue-Sheng Wang, Yan-Feng Wang, Hong-Tao Zhou, and Si-Min Yuan. Design of acoustic/elastic phase gradient metasurfaces: principles, functional elements, tunability, and coding. *Applied Mechanics Reviews*, 74(2):020801, 2022.

[8] Dongan Liu, Limei Hao, Weiren Zhu, Xiao Yang, Xiaole Yan, Chen Guan, You Xie, Shaofang Pang, and Zhi Chen. Recent progress in resonant acoustic metasurfaces. *Materials*, 16(21):7044, 2023.

[9] Ali Zabihi, Chadi Ellouzi, and Chen Shen. Tunable, reconfigurable, and programmable acoustic metasurfaces: A review. *Frontiers in Materials*, 10:1132585, 2023.

[10] Viktar S Asadchy, Mohammad Albooyeh, Svetlana N Tcvetkova, Ana Díaz-Rubio, Younes Ra'di, and SA Tretyakov. Perfect control of reflection and refraction using spatially dispersive metasurfaces. *Physical Review B*, 94(7):075142, 2016.

[11] Ana Díaz-Rubio and Sergei A Tretyakov. Acoustic metasurfaces for scattering-free anomalous reflection and refraction. *Physical Review B*, 96(12):125409, 2017.

[12] Mu Jiang, Yan-Feng Wang, Badreddine Assouar, and Yue-Sheng Wang. Scattering-free modulation of elastic shear-horizontal waves based on interface-impedance theory. *Physical Review Applied*, 20(5):054020, 2023.

[13] Junfei Li, Ailing Song, and Steven A Cummer. Bianisotropic acoustic metasurface for surface-wave-enhanced wavefront transformation. *Physical Review Applied*, 14(4):044012, 2020.

[14] Yu-Ze Tian, Yan-Feng Wang, Vincent Laude, and Yue-Sheng Wang. Generalized acoustic impedance metasurface. *Communications Physics*, 7(1):34, 2024.

[15] Junfei Li, Ana Díaz-Rubio, Chen Shen, Zhetao Jia, Sergei Tretyakov, and Steven Cummer. Highly efficient generation of angular momentum with cylindrical bianisotropic metasurfaces. *Physical Review Applied*, 11(2):024016, 2019.

[16] Xiuyuan Peng, Junfei Li, Chen Shen, and Steven A Cummer. Efficient scattering-free wavefront transformation with power flow conformal bianisotropic acoustic metasurfaces. *Applied Physics Letters*, 118(6):061902, 2021.

[17] Hong-Tao Zhou, Wen-Xiao Fu, Xiao-Shuang Li, Yan-Feng Wang, and Yue-Sheng Wang. Loosely coupled reflective impedance metasurfaces: Precise manipulation of waterborne sound by topology optimization. *Mechanical Systems and Signal Processing*, 177:109228, 2022.

[18] Haoyi Cheng, Jingwen Guo, Xin Zhang, and Wenjing Ye. Frequency-multiplexed transmitted-wave manipulation with multifunctional acoustic metasurfaces. *Physical Review Applied*, 20(3):034009, 2023.

[19] Yu-Ze Tian, Xiao-Lei Tang, Yan-Feng Wang, Vincent Laude, and Yue-Sheng Wang. Annular acoustic impedance metasurfaces for encrypted information storage. *Physical Review Applied*, 20(4):044053, 2023.

[20] Ana Díaz-Rubio, Junfei Li, Chen Shen, Steven A Cummer, and Sergei A Tretyakov. Power flow–conformal metamirrors for engineering wave reflections. *Science Advances*, 5(2):eaau7288, 2019.

[21] Junfei Li, Chen Shen, Ana Díaz-Rubio, Sergei A Tretyakov, and Steven A Cummer. Systematic design and experimental demonstration of bianisotropic metasurfaces for scattering-free manipulation of acoustic wavefronts. *Nature Communications*, 9(1):1–9, 2018.

[22] Hong-Tao Zhou, Shi-Wang Fan, Xiao-Shuang Li, Wen-Xiao Fu, Yan-Feng Wang, and Yue-Sheng Wang. Tunable arc-shaped acoustic metasurface carpet cloak. *Smart Materials and Structures*, 29(6):065016, 2020.

[23] Shi-Wang Fan, Sheng-Dong Zhao, Liyun Cao, Yifan Zhu, A-Li Chen, Yan-Feng Wang, Krupali Donda, Yue-Sheng Wang, and Badreddine Assouar. Reconfigurable curved metasurface for acoustic cloaking and illusion. *Physical Review B*, 101(2):024104, 2020.

[24] Shi-Wang Fan, Yan-Feng Wang, Liyun Cao, Yifan Zhu, A-Li Chen, Brice Vincent, Badreddine Assouar, and Yue-Sheng Wang. Acoustic vortices with high-order orbital angular momentum by a continuously tunable metasurface. *Applied Physics Letters*, 116(16):163504, 2020.

[25] Shi-Wang Fan, Yifan Zhu, Liyun Cao, Yan-Feng Wang, A-Li Chen, Aurélien Merkel, Yue-Sheng Wang, and Badreddine Assouar. Broadband tunable lossy metasurface with independent amplitude and phase modulations for acoustic holography. *Smart Materials and Structures*, 29(10):105038, 2020.

[26] Xiao-Shuang Li, Hong-Tao Zhou, Yan-Feng Wang, and Yue-Sheng Wang. Modulation of acoustic self-accelerating beams with tunable curved metasurfaces. *Applied Physics Letters*, 118(2):023503, 2021.

[27] Kemeng Gong, Xin Zhou, and Jiliang Mo. Continuously tuneable acoustic metasurface for high order transmitted acoustic vortices. *Smart Materials and Structures*, 31(11):115001, 2022.

[28] Jin He, Qingxuan Liang, Peiyao Lv, Yutao Wu, and Tianning Chen. Tunable broadband multi-function acoustic metasurface by nested resonant rings. *Applied Acoustics*, 197:108957, 2022.

[29] Ye Tian, Qi Wei, Ying Cheng, and Xiaojun Liu. Acoustic holography based on composite metasurface with decoupled modulation of phase and amplitude. *Applied Physics Letters*, 110(19):191901, 2017.

[30] Yong Li, Xue Jiang, Bin Liang, Jian-chun Cheng, and Likun Zhang. Metascreen-based acoustic passive phased array. *Physical Review Applied*, 4(2):024003, 2015.

[31] Yong Li, Chen Shen, Yangbo Xie, Junfei Li, Wenqi Wang, Steven A Cummer, and Yun Jing. Tunable asymmetric transmission via lossy acoustic metasurfaces. *Physical Review Letters*, 119(3):035501, 2017.

[32] Kun Tang, Chunyin Qiu, Manzhu Ke, Jiuyang Lu, Yangtao Ye, and Zhengyou Liu. Anomalous refraction of airborne sound through ultrathin metasurfaces. *Scientific Reports*, 4(1):6517, 2014.

[33] Yangbo Xie, Wenqi Wang, Huanyang Chen, Adam Konneker, Bogdan-Ioan Popa, and Steven A Cummer. Wavefront modulation and subwavelength diffractive acoustics with an acoustic metasurface. *Nature Communications*, 5(1):5553, 2014.

[34] Yu-Chi Su and Li-Heng Ko. Acoustic wave splitting and wave trapping designs. *Journal of Vibration and Acoustics*, 144(3):034502, 2022.

[35] Yanlong Xu, Liyun Cao, Pai Peng, Xiaoling Zhou, Badreddine Assouar, and Zhichun Yang. Beam splitting of flexural waves with a coding meta-slab. *Applied Physics Express*, 12(9):097002, 2019.